Effects of realistic inflow conditions on the aero-thermal performance of a film-cooled vane

Proceedings of
11th European Conference on Turbomachinery Fluid dynamics & Thermodynamics
ETC11, March 23-27, 2015, Madrid, Spain

EFFECTS OF REALISTIC INFLOW CONDITIONS ON THE AERO-THERMAL PERFORMANCE OF A FILM-COOLED VANE

M. Insinna - D. Griffini - S. Salvadori[1] *- F. Martelli*

Department of Industrial Engineering (DIEF), University of Florence
via S. Marta 3, 50139 Florence, Italy

ABSTRACT

A high-pressure vane equipped with a realistic film-cooling configuration has been studied. The vane is characterized by the presence of multiple rows of fan-shaped holes along pressure and suction side while the leading edge is protected by a showerhead system of cylindrical holes. Steady three-dimensional Reynolds-Averaged Navier-Stokes simulations have been performed. A preliminary grid sensitivity analysis has been performed with uniform inlet flow to quantify the effect of the spatial resolution. Turbulence model has been assessed in comparison with available experimental data. The effects of a realistic inflow condition on the thermal behaviour of the cooled vane are then investigated by means of comparison between two conjugate heat transfer simulations. The first one is characterized by a uniform inlet flow while the second one presents a temperature distortion and a superimposed aggressive swirl derived from the EU-funded TATEF2 project. The effect of the swirling flow in determining the metal temperature distribution is investigated with particular attention to the consequences on the operation of the film cooling system.

NOMENCLATURE

c_{ax}	$[m]$	axial chord
k_L	$[m^2/s^2]$	laminar kinetic energy
k_T	$[m^2/s^2]$	turbulent kinetic energy
L	$[m]$	chord
Pr	$[-]$	Prandtl number
$\dot{Q}$	$[W]$	thermal power
$\dot{q}$	$[W/m^2]$	heat flux
s	$[m]$	curvilinear coordinate
T	$[K]$	temperature
u	$[m/s]$	velocity magnitude
y^+	[-]	non-dimensional wall distance
greek		
η	$[-]$	adiabatic effectiveness
ω	$[s^{-1}]$	turbulence specific dissipation rate
subscripts and superscripts		
0		stagnation quantity
c		referred to coolant
in		referred to inlet quantity
is		isentropic
m		referred to main-flow
rec		recovery
$\overline{[\,]}$		averaged quantity
$\widetilde{[\,]}$		pitchwise averaged quantity
$\widehat{[\,]}$		spanwise averaged quantity

[1]corresponding author: office: +39 055 2758 779, email: simone.salvadori@unifi.it

INTRODUCTION

The continuous demand for increased performance and reliability of gas turbines requires detailed analysis of aero-thermal aspects that characterize the coupling between combustion chamber and High-Pressure Vane (HPV). Flame stabilization in modern gas turbine combustors needs strong swirl motion, which is conserved up to the entrance of the turbine. Moreover, the intrinsic complexity of the flow field inside of the combustion chamber generates non-uniform conditions on the turbine inlet section in terms of thermal field and turbulence level. All these aspects govern the thermal load on metal parts. Having regard to the effects of heat transfer on the residual life of gas turbine components, a high level of accuracy in the evaluation of thermal loads is necessary. For this reason realistic inlet boundary conditions should be used to analyze thermal field in metal components. One of the most challenging topics in Computational Fluid Dynamics (CFD) is the numerical simulation of a cooled transonic HPV. It includes the analysis of a transitional flow governed by geometrical parameters and by strong compressibility effects. Furthermore, very different geometrical length scales are a peculiar characteristic of this kind of geometry. Referring to the works of Gourdain *et al*. (2011) and Duchaine *et al*. (2009), Large Eddy Simulation (LES) has been recently used for the aero-thermal analysis of HPV. Such a demanding approach entail the disadvantage to result not serviceable during an industrial design procedure. A less demanding approach based on the Detached-Eddy Simulation (DES) has been proposed by Takahashi *et al*. (2012) showing good results when applied to a simplified leading edge configuration with showerhead cooling. However, DES performance in a realistic HPV environment has still to be analyzed. The traditional approach to the analysis of the heat transfer in a cooled HPV consists in steady or unsteady simulations where turbulence is modeled using two-equation approaches. Adami *et al*. (2003) demonstrate that the low-Reynolds k-ω model by Wilcox (1993) is able to reproduce the Nusselt number distribution on the blade surface with reasonable accuracy. Improvements in the Nusselt number evaluation are expected when modeling boundary layer transition. Luo and Razinsky (2007) present the numerical study of an internally cooled vane using a Conjugate Heat Transfer (CHT) approach and the k-ϵ-ν^2-f transition model by Lien and Kalitzin (2001). Results compared with experimental data show good agreement at least for this simplified test-case. In fact the vane geometry is equipped with internal cooling channels only and then no information is provided on film cooling effects. Insinna *et al*. (2014a) studied the ability of the transition k_T-k_L-ω model by Walters and Cokljat (2008) to deal with a film-cooled vane configuration using a CHT approach. A transition model assessment has also been performed and a new set of constants has been proposed. Obtained results showed a relevant effect of bypass transition in the Nusselt number evaluation of cooled configurations. The next step in the analysis of film-cooled, transonic HPV configuration with CHT approach is to include non-uniform inlet conditions representative of realistic working conditions. Such a detailed analysis would provide information of combustor/turbine interaction both on the performance of the cooling system and on the thermal field. This has been accomplished by Insinna *et al*. (2014a) on a research HPV with a simplified cooling system.

The present work deals with the study of the test rig described by Jonsson and Ott (2007) with inlet non-uniformities representative of a real combustor. The use of the k_T-k_L-ω with modified parameters and a grid dependence analysis ensure a reliable analysis. The main feature of this work is the external cooling system that is representative of modern turbine design. Cooling system performance are evaluated as well as thermal fields of both blades and end-walls.

DESCRIPTION OF THE TEST CASE

A detailed description of the selected test case is available in the research papers by Jonsson and Ott (2007) and Charbonnier *et al*. (2008). It is a transonic research vane experimentally investigated with uniform inflow in a linear cascade at the École Polytechnique Fédérale de Lausanne during the

	Main	Coolant	Outlet
inlet total temperature $[K]$	333	303	
inlet total pressure $[bar]$	1.535	1.780	
inlet total pressure $[K]$	333	303	
inlet turbulence level $[\%]$	10	5	
inlet turbulent length scale $[m]$	0.013	0.0004	
static pressure $[bar]$			0.927

Table 1: **Boundary conditions (experimental configuration)**

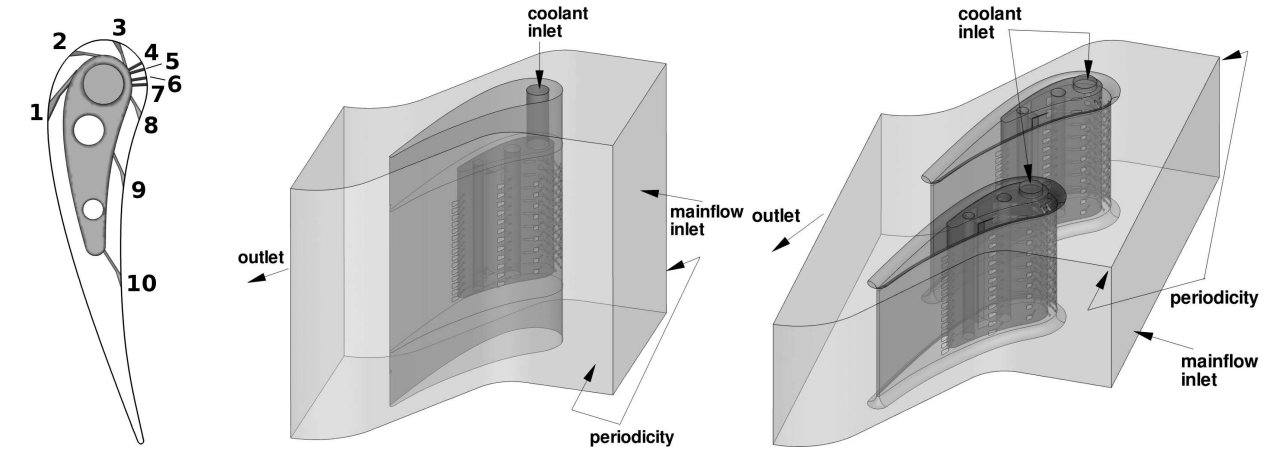

(a) cooling system (b) experimental configuration (c) engine-like configuration

Figure 1: **Schematic of the cooling system and computational domains**

EU-funded TATEF2 project. The Reynolds number, based on the true chord and evaluated at the outlet section, is $1.46 \cdot 10^6$ while the value of the isentropic exit Mach number is 0.88. The cooling system is shown in Figure 1(a) and consists of three rows of fan-shaped holes on both suction and pressure side and four rows of cylindrical holes inclined downward by $45°$ on the leading edge (showerhead). CO_2 is used as coolant to provide a coolant-to-main-flow density ratio of about 1.7, which is representative of engine-like conditions. The nominal blowing ratio of the showerhead holes is about 2.8, while for the rows from 1 to 3 it is in the range $1 \div 1.5$ and varies from 3.4 to 1.5 passing from row 8 to row 10. More details on the non-dimensional parameters of the cooling system are given by Jonsson and Ott (2007). Operating conditions are summarized in Table 1.

Experimental geometry

The computational domain used for grid sensitivity analysis and turbulence model assessment reproduces the experimental configuration of Jonsson and Ott (2007) (Figure 1(b)). It contains the whole fluid region including coolant channels and plenum. Inlet and outlet sections are placed respectively about $0.65c_{ax}$ upstream of the leading edge and about $0.60c_{ax}$ downstream of the trailing edge. The inlet section of the cooling flow is located on top of the cascade. Total pressure, total temperature, turbulence level, turbulent length scale and flow direction have been imposed on inlet sections for all the simulation. For the heat flux computation an isothermal boundary condition has been imposed along the walls ($323K$ according to Charbonnier *et al*. (2008)), while the adiabatic condition has been used for the evaluation of adiabatic effectiveness.

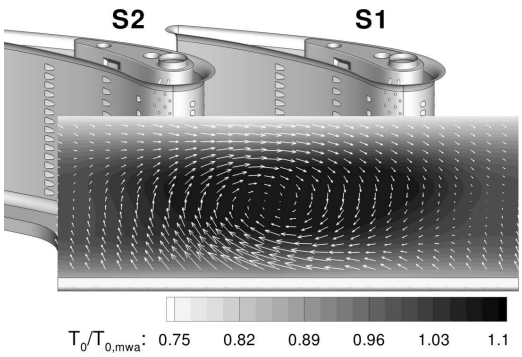

(a) relative alignment of hot spot and swirl with respect to the vanes

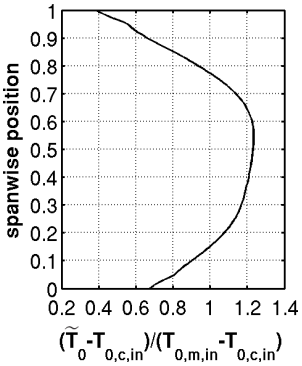

(b) pitchwise averaged non-dimensional total temperature profile

Figure 2: **Non-uniform inlet conditions**

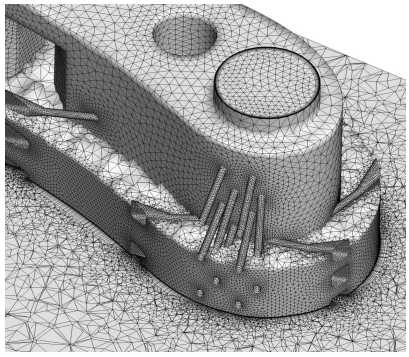

Figure 3: **Computational mesh (engine-like case)**

Realistic geometry and inflow conditions

Concerning the study of the effects of inlet swirl and hot spot, a modified domain with two passages has been generated using the same cooling system with a reduced aspect ratio (Figure 1(c)), in order to be representative of a real machine configuration. For the same reason when performing conjugate simulations a metal conductivity of 11 W/mK has been selected resulting in a Biot number of 0.5. The hot spot and swirl profiles derives from the experimental campaign of the EU-funded TATEF2 project and are respectively described in the works by Salvadori *et al*. (2011) and by Qureshi *et al*. (2012). The relative alignment between hot spot and vane passage is shown in Figure 2(a). The swirl core is aligned with respect to the hot spot and both of them are centered with respect to the vane passage. The hot spot profile is colloquially referred form the TATEF2 project as "EOTDF" (Enhanced Overall Temperature Distortion Factor). The pitchwise averaged non-dimensional total temperature profile is reported in Figure 2(b). Considering pitchwise averaged and spanwise averaged temperature profiles, the non-uniformities are characterized by the difference between maximum and minimum peaks calculated in equations 1a and 1b.

$$\textit{spanwise non-uniformity:} \qquad \left(\widetilde{T}_{0,max} - \widetilde{T}_{0,min}\right) \Big/ \overline{T_0} = 0.355 \tag{1a}$$

$$\textit{pitchwise non-uniformity:} \qquad \left(\widehat{T}_{0,max} - \widehat{T}_{0,min}\right) \Big/ \overline{T_0} = 0.14 \tag{1b}$$

It is evident that the non-uniformity is mainly in the spanwise direction, coherently with modern aero-engines.

In order to maintain coherency between the minimum total temperature of the non-uniform inlet profile and the coolant total temperature, this latter has been reduced for the engine-like case reaching a coolant-to-main-flow ratio of 0.598 with the main-flow total temperature unaltered. Moreover, air is used as coolant without modifying its inlet pressure, obtaining a nominal density ratio equal to the one of the experimental configuration.

All the simulations performed are summarized in Table 2.

	Domain	Cooling	Thermal B.C.	Inlet conditions
grid sensitivity analysis	experimental	yes	$323K$	uniform
evaluation of $\widehat{\eta}$ (validation)	experimental	yes	adiabatic	uniform
evaluation of $\widehat{\dot{q}}$ (validation)	experimental	yes	$323K$	uniform
evaluation of isentropic Mach (validation)	experimental	no	$323K$	uniform
reference case	engine-like	yes	CHT	uniform
realistic inflow	engine-like	yes	CHT	EOTDF+swirl

Table 2: **Test matrix**

NUMERICAL APPROACH AND MODEL VALIDATION

Numerical method

Numerical simulations on hybrid unstructured grids have been performed using a steady approach with the commercial code ANSYS® Fluent. The k_T-k_L-ω transitional model by Walters and Cokljat (2008) has been selected for turbulence closure. A second-order accurate upwind discretization has been applied in space, while gradients are reconstructed with the Green-Gauss node based approach.

Model validation

Grid dependence analysis

In order to ensure a reliable analysis, a preliminary grid sensitivity analysis has been performed on the experimental configuration to evaluate spatial discretization effects on the numerical solution. Hybrid unstructured grids generated with the commercial software Centaur™ have been generated. Prismatic layers are used near the walls to improve the boundary layer profile reconstruction while tetrahedra fill the remaining volume. Refinements have been enforced both in the cooling channels and in the mixing zone between cooling flow and mainstream. Four different grids have been generated consisting of about 3.66M, 6.35M, 14.2M and 25.9M elements. For all the grids the number of prismatic layers and their height are maintained unchanged in order to maintain the accuracy in the discretization of boundary layer. That choice results in a average y^+ value of 0.3 while its maximum volue is about 0.92. Negligible variations have been observed in terms of pressure field. Grid effects have been quantified for the mass-flows, total pressure losses and average heat flux using the Grid Convergence Index (GCI) suggested by Roache *et al*. (1986). The GCI value on the fine mesh is 1.18% for coolant mass-flow, 0.45% for loss coefficient and 2.92% for the average heat flux. It can be concluded that increasing the computational cost from 14.2M elements to 25.9M the solution variation is limited and then the 14.2M grid has been selected for the subsequent simulations. Once the distribution of grid dimensions have been assessed, it has also been applied to the engine-like configuration, obtaining the grid shown in Figure 3 (composed by about 37M elements including the solid parts).

Assessment of the turbulence model

The assessment of the turbulence model has been performed on the experimental configuration with uniform inlet flow, comparing three different approaches. The fully turbulent SST k-ω has been compared with the k_T-k_L-ω transition model by Walters and Cokljat (2008) with standard parameters and with a re-calibrated version of this latter proposed in the work by Insinna *et al*. (2014a) and Insinna *et al*. (2014b). Model tuning has been performed on a different cooled HPV.

The k_T-k_L-ω is based on the k-ω structure but is able to predict both natural and bypass transition mechanisms thanks to a third transport equation for the so-called laminar kinetic energy k_L that predicts the behavior of the low-frequency velocity fluctuations in the pre-transitional zones. Ap-

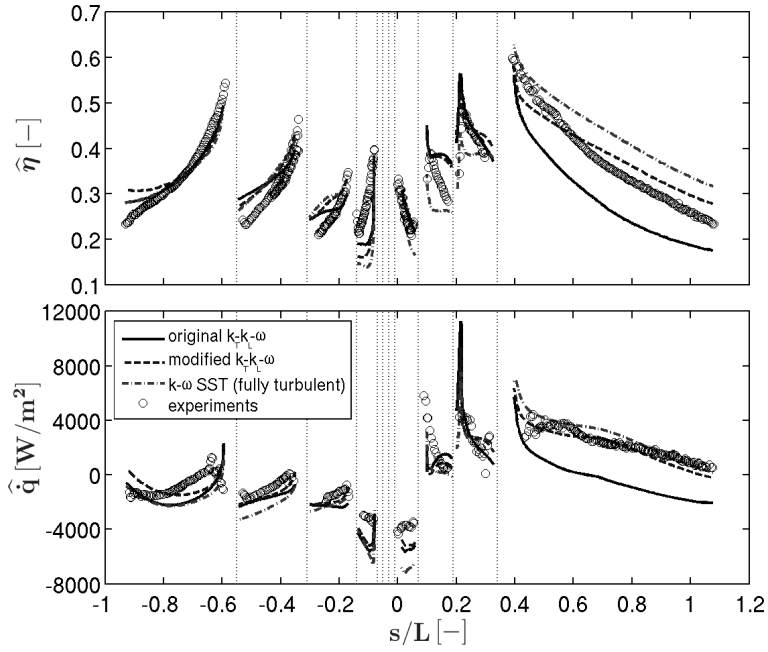

Figure 4: **Effect of turbulence model (pressure side for $\mathbf{s/L < 0}$)**

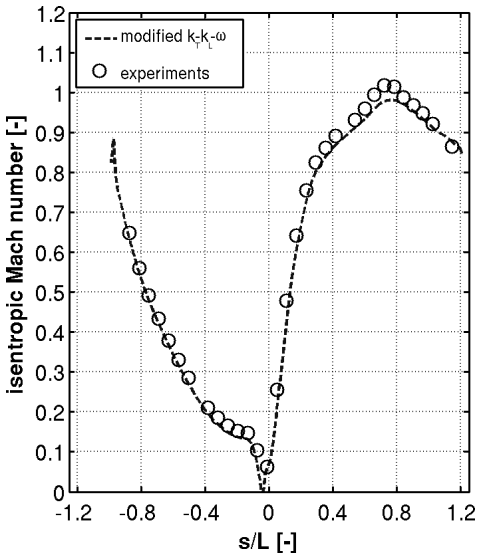

Figure 5: **Isentropic Mach number (midspan of uncooled experimental geometry)**

propriate production and dissipation terms act the kinetic energy transfer between k_L and k_T in the transport equations of the model, allowing to reproduce by-pass and natural transition. Film cooling rows are then not considered as a local "artificial" source for triggering transition but the integration of the transport equations of k_L and k_T allows considering the kinetic energy transfer between k_L and k_T downstream of the holes, as well as throughout the rest of the domain.

Results, in terms of the spanwise-averaged adiabatic effectiveness (defined in equation 2, where $\widehat{T}_{rec,m}$ is calculated on the uncooled vane) and heat flux are compared with the available experimental data.

$$\widehat{\eta} = \frac{\widehat{T}_{rec,m} - \widehat{T}_{aw}}{T_{0,m,in} - T_{0,c,in}} \qquad \text{where:} \qquad \widehat{T}_{rec,m} = \widehat{T}_m + Pr^{\frac{1}{3}} \frac{\widehat{u}^2_{m,is}}{2c_p} \tag{2}$$

It must be underlined that heat flux data are analyzed for a different working condition with respect to what reported in Table 1: the main-flow inlet total pressure is equal to $1.493bar$ (with the isentropic Mach number unchanged) and a coolant mass-flow is $6.8g/s$, coherently to the work of Charbonnier *et al*. (2008). The local heat flux at the wall is defined in equation 3

$$\dot{q} = -k \left. \frac{\partial T}{\partial n} \right|_w \tag{3}$$

where k is the thermal conductivity of the fluid and the partial derivative of temperature in direction normal to the wall (n) is calculated assuming normal unity vector entering the fluid itself. With such definition, it follows that heat flux is positive when fluid is heated.

As shown in Figure 4, a general good agreement between the qualitative trends of predictions and experiments is achieved. Comparing the turbulence models, different behaviors are shown downstream of the cooling rows (represented by vertical dotted lines). From a quantitative point of view turbulence models are mainly discordant downstream of the last cooling row on the suction side

($s/L > 0.4$), where the SST k-ω over-predicts $\widehat{\eta}$ while the original k_T-k_L-ω significantly under-predicts $\widehat{\eta}$. A similar behavior is also evident for heat flux. In that region the modified k_T-k_L-ω proposed by Insinna *et al*. (2014a) shows the best performance. Looking also at the other zones, the modified k_T-k_L-ω demonstrates to be a good compromise for the prediction of both effectiveness and heat flux. In order to quantify the errors of the compared turbulence models an evaluation point has been selected at $s/L = 0.7$. The reason for the choice of this position is that fact that at that point turbulence models show their maximum disagreement. In terms of span-wise adiabatic effectiveness, using as a reference the experimental value, the re-calibrated $k_T - k_L - \omega$ gives a $+8\%$ difference, the original $k_T - k_L - \omega$ a -26% difference and the fully turbulent model a $+21\%$ difference. Instead, in terms of span-wise wall heat flux the same turbulence models gives respectively $+7\%$, -113% and $+35\%$ difference. Therefore, the re-calibrated $k_T - k_L - \omega$ has been selected for the subsequent simulations.

The three turbulence models have been used also to reproduce the aerodynamic field of the uncooled geometry, for which experimental data is available in terms of isentropic Mach number. Same boundary conditions shown in Table 1 have been used for the main flow. Geometry is the same of Figure 1(b), except for the absence of the cooling system. Results are presented in Figure 5 for the modified k_T-k_L-ω model only since negligible variations have been observed with the other turbulence closures tested. A general good agreement is obtained, except for $0.6 < s/L < 0.8$ on the suction side where the isentropic Mach number is slightly under-estimated (-4.5% at $s/L = 0.75$). Same behavior has been observed in the work of Charbonnier *et al*. (2008) with the SST k-ω turbulence model. The underestimation of Mach number on suction side could be ascribed to the steady approach that does not correctly reproduce the effect of the unsteady vortex shedding downstream of the trailing edge.

EFFECTS OF THE REALISTIC INFLOW CONDITIONS

Thermal fields of the solid parts

Figure 6 shows the thermal fields along the metal parts both for the uniform and non-uniform inlet cases. A first aspect immediately visible from Figure 6 is that, when uniform inflow is considered, end-walls are hotter than in case of non-uniform inlet profile. It can be explained considering that temperature non-uniformity is mainly in spanwise direction and then end-walls are not affected by the high temperature level of the hot spot. In case of uniform inlet profile the increased thermal load along the end-walls highlights the heat sink effect in proximity of the coolant inlet, which is positioned on the upper end-wall. That outcome is less evident in the EOTDF+swirl case. For this latter, looking at the surfaces of the vanes, the temperature increase at mid-span appears lower than expected along most of the surfaces. This indicates that the cooling system remains effective enough to mitigate the effect of the hot spot, especially in the front part of the vanes. However it must be underlined that a quite extended zone in the lower-rear part of the S2 vane undergoes a strong temperature increase with respect to the uniform case (see Figures 6(c) and 6(d)). A detailed investigation demonstrates that the overheating is caused by two effects: the hot spot migration inside of the passage and the film cooling effectiveness reduction in the rear part of the suction side of the S2 vane. Hot spot migration inside of the vane drives the hot core to the S2 vane suction side where strong aerodynamic effects caused by swirl reduce the coverage provided by the cooling system. Looking at Figure 7 the effects of swirl in altering the aerodynamic load of the vanes can be clearly individuated. Comparing the isentropic Mach number distributions at 15% and 85% of the span of the vanes for the uniform and the EOTDF+swirl cases it is evident that swirl affects mainly the S2 vane, causing a strong negative incidence near hub and a strong positive incidence near casing. It follows that the behaviour of the film cooling system in terms of coverage is considerably altered, leading to the already mentioned deleterious consequences along the suction side of the S2 vane.

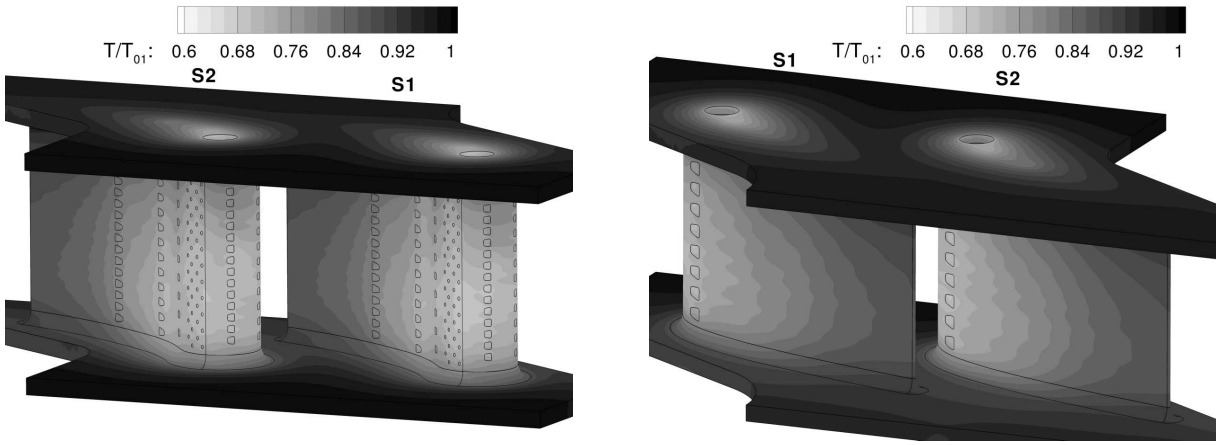

(a) uniform inlet (front view)

(b) uniform inlet (rear view)

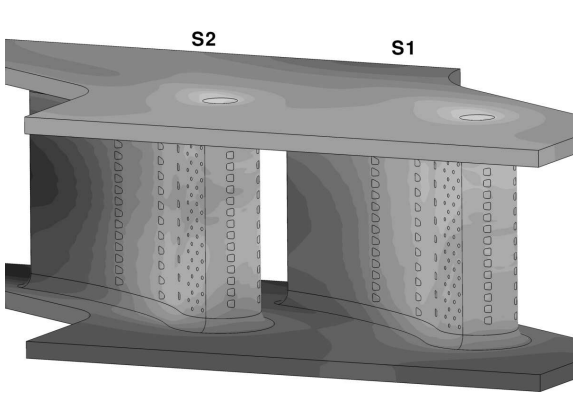

(c) EOTDF+swirl (front view)

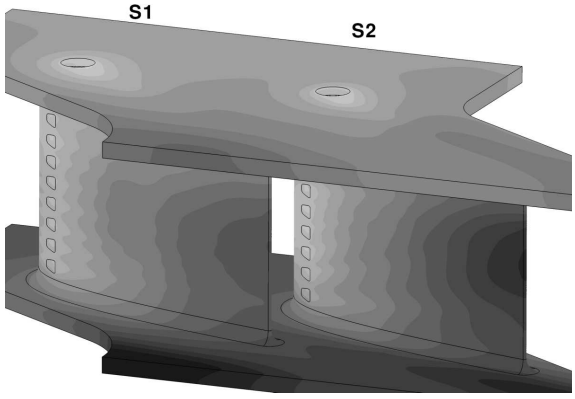

(d) EOTDF+swirl (rear view)

Figure 6: **Temperature fields along vanes and end-walls**

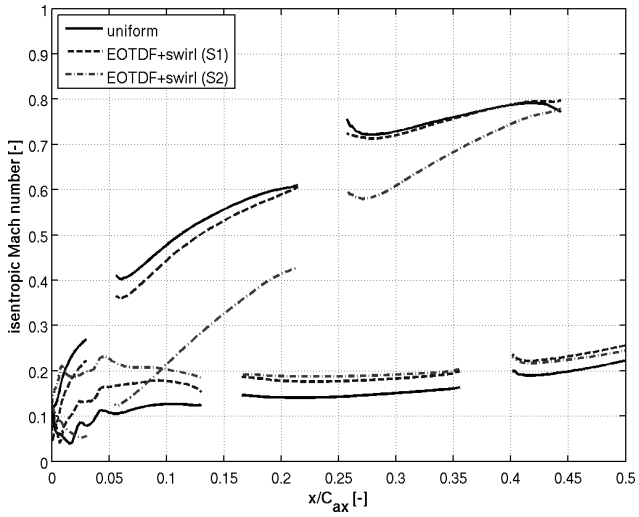

(a) 15% span

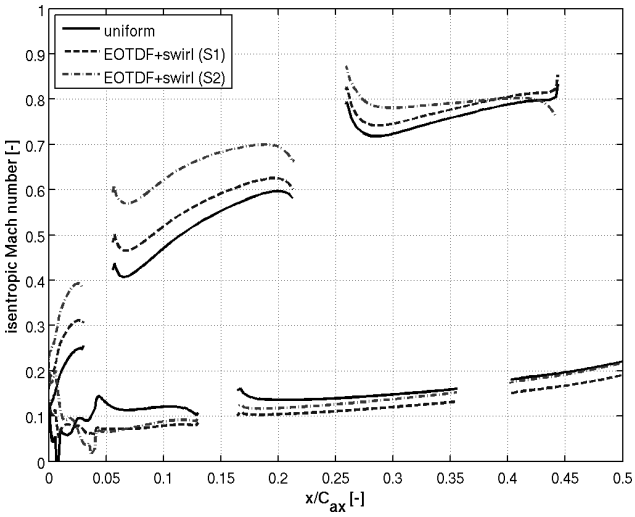

(b) 85% span

Figure 7: **Isentropic Mach number distributions in the front part of the vanes**

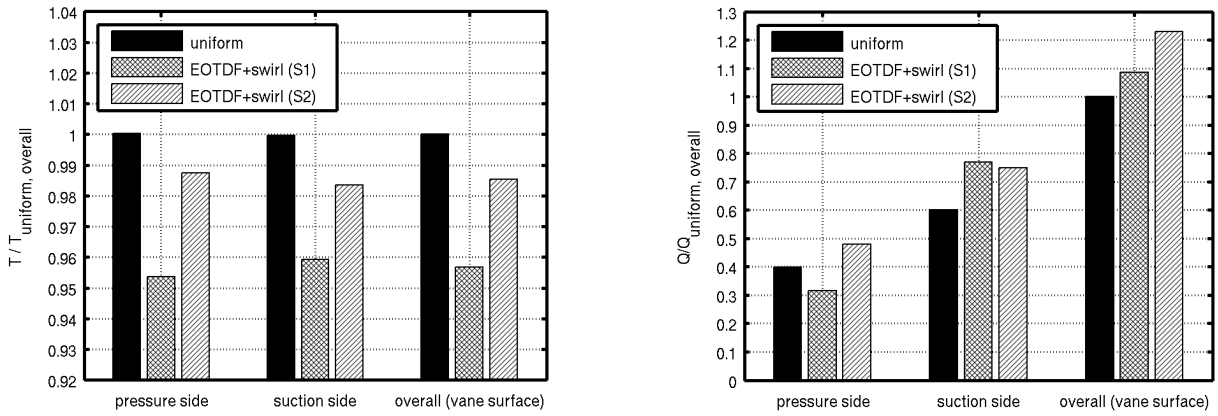

(a) non-dimensional average temperature

(b) non-dimensional thermal power

Figure 8: **Average temperatures and distributions of the thermal load (normalization is calculated with respect to the overall data of the uniform case).**

Figure 8 reports the non-dimensional averaged temperature and thermal power for pressure and suction side (including fillets) as well as the overall data. This latter includes only the external vane surfaces without considering platforms. The thermal power $\dot{Q}$ is defined in equation 4 as the discretized surface integral of the local heat flux (defined in equation 3)

$$\dot{Q} = \sum_i \dot{q}_i A_i \tag{4}$$

where i is the index of the surface element on the considered zone and A_i its area.

Although the maximum temperature peaks are higher in the non-uniform case, Figure 8(a) shows that the uniform inlet flow generates higher average temperatures. The other aspect that emerges, coherently with what discussed above, is that the S2 vane in the EOTDF+swirl case is characterized by higher temperature levels with respect to the S1, due to aerodynamic alteration of the film cooling system and to the hot spot migration. Analyzing Figure 8(b), where the thermal power transferred from fluid to metal is shown, an overall increase of the thermal power is observed for the EOTDF+swirl case with respect to the uniform case. As previously stated, an opposite behavior is highlighted in terms of temperature. Such a behavior can be linked to internal heat conduction from end-walls to vanes due to higher temperature of the first ones in the uniform case. In order to quantify its effect, a thermal balance on the metal domain of each vane has been considered. A schematic of the control volume used is shown in Figure 9. Such domain accounts for conductive fluxes from the end-walls and convective fluxes from the external (pressure side (PS) and suction side (SS)) and internal vane surfaces (plenum and cooling channels). Thermal power, reported in Table 3, has been considered referring to the metal of the vane. In such convention, a positive thermal power increases metal temperature while a negative one is representative of a cooling effect. From Table 3 it is possible to deduce that, in the uniform case, the 35.2% of the total exiting heat is removed through the surfaces of the cooling channels while the remaining 64.8% from the plenum. Both such contributions are due to convective fluxes. The heat entering the vane is redistributed as follow: 71.6% is due to convective fluxes through the external vane surfaces (PS and SS) while the remaining 28.4% is due to thermal conduction from the end-walls. This latter data allows understanding the major role of conduction in the thermal balance of the vanes and can not be considered without a conjugate heat transfer analysis. As expected, slight variations are encountered for internal convective fluxes (plenum and cooling

channels) when comparing the uniform case with the EOTDF+swirl one. A maximum variation of -6.8% with respect to the total cooling effect of the uniform case is highlighted for the plenum in the S1 vane and a $+2.5\%$ for the cooling channels in the S2 vane. The maximum variations for the positive thermal power, referred to the total heating effect of the uniform case, are encountered in the S2 vane with an increase of $+16.4\%$ for the external vane surfaces and a -19.4% for the conductive flux. This latter is due to the end-walls cooling provided by the EOTDF temperature profile (the average inlet temperature of the main-flow is the same for uniform and EOTDF+swirl cases). The apparent inconsistency between average temperatures (Figure 8(a)) and thermal loads (Figure 8(b)) is explained by the effect of thermal conduction. In spite of an increase of external thermal load ($+8.5\%$ and $+22.8\%$ respectively for S1 and S2 vanes having the uniform case as a reference), the overall vane temperature decreases mainly due to the strong reduction of the conductive heat fluxes from the end-walls (-50.1% and -68.4% respectively for S1 and S2 vanes having the uniform case as a reference).

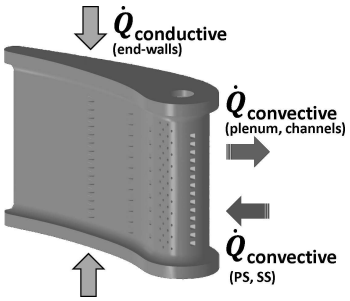

Figure 9: **Schematic of thermal balance on the vane control volume**

	uniform	**EOTDF+swirl**	
		S1 vane	***S2 vane***
channels	-52.9	-51.0	-56.6
PS+SS	107.7	116.9	132.3
plenum	-97.5	-87.2	-89.2
end-walls	42.7	21.3	13.5

Table 3: **Thermal power ($\dot{Q}$ [W]) balance on the vane (control volume shown in Figure 9)**

Behaviour of the showerhead cooling rows

The leading edge region of a HPV is critical from a thermal point of view due to the strong curvature of the surface that makes almost impossible to generate an attached film of coolant. For this reason the use of showerhead holes, where a large amount of heat is removed through heat sink effect, is a constrained choice. Realistic inlet flows are characterized by strong swirl velocity components that alter sensibly the pressure distribution in the front part of the vanes, as previously shown in Figure 7. For this reason the behaviour of such cooling systems are particularly problematic and a detailed analysis of the operation of the showerhead is presented here.

Figure 10(a) reports the thermal power (defined in equation 4) removed along the internal surface of each showerhead hole, grouping the holes by rows (see Figure 1(a)). Before to comment the effects of the non-uniform inlet profile some considerations should be done about the uniform case looking at Figure 10(a). All the rows show a bow-shaped distribution of $\dot{Q}$ due to the heat flux coming from the end-walls, where an adiabatic condition has been imposed on the top and bottom metal surfaces. The bow-shaped behaviour of the rows 5 and 7 is slightly distorted in the upper part because these two rows are shifted upward by half a hole pitch and are closer to the upper end-wall with respect to rows 4 and 6.

The effects of the non-uniform inlet profile in determining $\dot{Q}$ is remarkable both observing the differences with respect to the uniform case and the differences between S1 and S2 vanes. The bow-shaped distribution is no more valid for the EOTDF+swirl case due to the reduced temperature of the end-walls (see Figure 6) and the consequently reduced heat flux coming from them. Despite quantitative differences, a similar pattern between the distributions of $\dot{Q}$ of the four rows for the non-

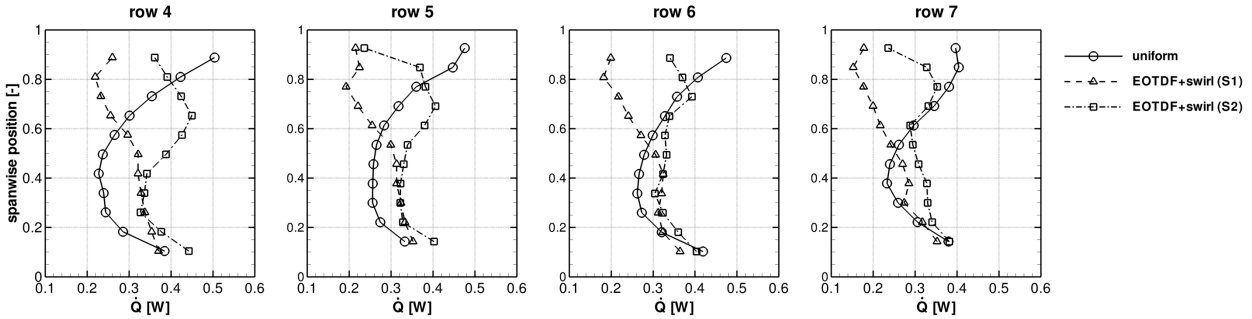

(a) thermal power

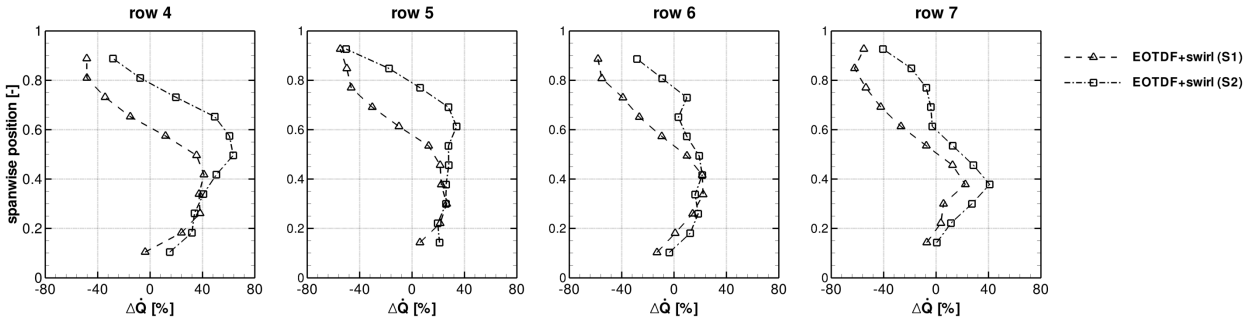

(b) thermal power difference between uniform and EOTDF+swirl

Figure 10: **Thermal power exchanged by the showerhead holes by heat sink effect (the two vanes are shown for the EOTDF+swirl case)**

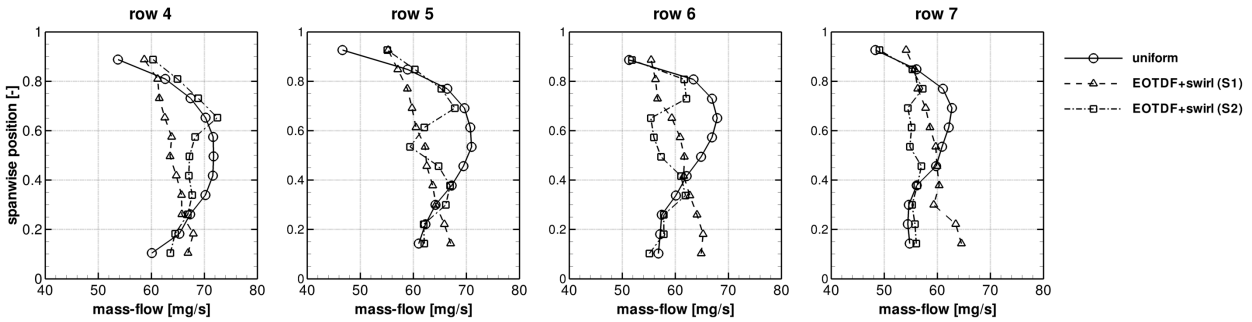

(a) mass-flow

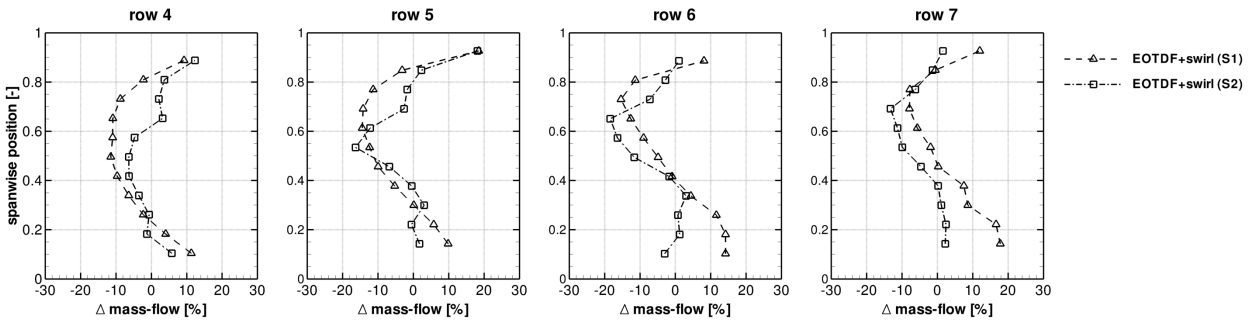

(b) mass-flow difference between EOTDF+swirl and uniform

Figure 11: **Mass-flow of the showerhead holes (the two vanes are shown for the EOTDF+swirl case)**

uniform case is shown in Figure 10(b), where the percentage difference with respect to the uniform case is shown. Figure 10(b) allows also to clearly observe that the holes exchange less thermal power with respect to the uniform case in the upper part of span as a consequence of the radial temperature distribution of the inlet profile. The maximum and minimum variations of thermal power obtained with the EOTDF+swirl profile are very high, confirming the particular sensitivity of the showerhead system to the inflow characteristics. They are respectively located at midspan of the S2 vane on the row 4 ($\Delta\dot{Q} \simeq +64\%$) and near casing of the S1 vane on the row 7 ($\Delta\dot{Q} \simeq -62\%$).

Figure 11 shows an analysis of the the mass-flow passing through the showerhead channels. As for the thermal power, the mass-flow of the channels, reported in Figure 11(a), is characterized by a bow-shaped distribution in the uniform inlet case although in the opposite sense. This behavior is due to the proximity of the upper and lower holes with the end-walls, which cause local effects of streamline curvature near the corners of the coolant plenum, reducing the mass-flow through that holes with respect to the holes located far from the end-walls. The effects of the non-uniform inlet profile in modifying the mass-flow distribution between the holes are very important. As it is possible to observe from Figure 11(b) for the non-uniform inlet case, through the lower part of the showerhead of the S2 vane, the amount of injected mass-flow is lower than for the corresponding zone of the other vane. That portion of span tends to increase its extension passing from row 4 to row 7, while the opposite happens in the upper part of the span, where an inversion of the mass-flow difference is visible. Furthermore, very high quantitative variations are present, although less intense than for the thermal power. In fact, the maximum reduction of the mass-flow, with respect to the uniform inlet case, is about -19% and is achieved on the S2 vane at 65% of the span while the maximum increase of the mass-flow is about 19% and is located near the upper end-wall of both the vanes.

CONCLUSIONS

Conjugate heat transfer analysis of a cooled transonic high-pressure vane has been performed. Simulations with inlet conditions representative of a realistic engine have been compared with uniform conditions in terms of aero-thermal characteristics.

The analysis of the thermal fields into the solid parts highlighted different temperature distribution on the end-walls between uniform inlet case and realistic inflow. Concerning the surfaces of the vanes, an high-temperature spot is located on S2 vane suction side due to the hot spot migration inside of the passage. The hot-streak migration is not the only factor that affects the S2 vane thermal field. in fact, on that vane, swirl aerodynamic effects are more aggressive than on the S1 vane, affecting coolant coverage.

Thermal behavior has been also analyzed in terms of average temperatures and thermal power along the surfaces of the vanes. Results show an opposite behavior of the uniform case with respect to the EOTDF+swirl one. Temperature on the vanes results to be higher in the uniform case while thermal power is lowered. This apparent incoherence find explanation from the analysis of internal conductivity through the end-walls. In fact, conductive heat flux passing from end-walls to vanes results to be strongly related to the inlet profile.

The analysis of the showerhead performance allowed to highlight some relevant effects. Bow-shaped distribution has been found for thermal power inside of the cooling channel in the uniform case due to the heat flux coming from the end-walls. A different distribution has been found for the EOTDF+swirl case due to the hot spot radial distribution reducing internal conduction. Variations ranging from -65% to $+75\%$ have been highlighted in terms of thermal power removed by heat sink effect. Concerning the coolant mass-flow injected from the showerhead, a bow-shaped distribution (opposite to the one observed for thermal power), has been found for the uniform case, showing a reduction near the end-walls. In terms of injected mass-flows, variations between uniform and EOTDF+swirl cases range from -19% to $+19\%$.

References

Adami P, Martelli F, Chana KS, Montomoli F, *Numerical predictions of film cooled NGV blades*, Proc. of IGTI, ASME Turbo Expo 2003, June 16-19, Atlanta, Georgia, US, Volume 5: Turbo Expo 2003, Parts A and B, Paper No. GT-2003-38861, pp. 639-649, doi: 10.1115/GT2003-38861

Charbonnier D, Ott P, Jonsson M, Köbke T, Cottier F, *Comparison of numerical investigations with measured heat transfer performance of a film cooled turbine vane*, Proc. of the ASME Turbo Expo 2008: Power for Land, Sea, and Air, Volume 4: Heat Transfer, Parts A and B, Berlin, Germany, June 9-13, pp. 571-582, doi: 10.1115/GT2008-50623.

Duchaine F, Corpron A, Pons L, Moureau V, Nicoud F, Poinsot T, *Development and assessment of a coupled strategy for conjugate heat transfer with large eddy simulation: application to a cooled turbine blade*, International Journal of Heat and Fluid Flow 2009, 30:1129-1141, doi: 10.1016/j.ijheatfluidflow.2009.07.004

Gourdain N, Gicquel LYM, Collado Morata E, *Comparison of RANS simulation and LES for the prediction of heat transfer in a highly loaded turbine guide vane*, Proc. of the Ninth European Conference on Turbomachinery - Fluid Dynamics and Thermodynamics 2011, March 21-25, Istanbul, Turkey, Paper No. B235

Insinna M, Griffini D, Salvadori S, Martelli F, *Conjugate heat transfer analysis of a film cooled high-pressure turbine vane under realistic combustor exit flow conditions*, Proc. of the ASME Turbo Expo 2014: Turbine Technical Conference and Exposition, Volume 5A: Heat Transfer, Dusseldorf, Germany, June 16-20, 2014, doi:10.1115/GT2014-25280

Insinna M, Griffini D, Salvadori S, Martelli F, *Film cooling performance in a transonic high-pressure vane: decoupled simulation and conjugate heat transfer analysis*, Energy Procedia, 45, 2014, pp. 1126-1135, doi: 10.1016/j.egypro.2014.01.118

Jonsson M, Ott P, *Heat transfer experiments on a heavily film cooled nozzle guide vane*, Proc. of the Seventh European Conference on Turbomachinery - Fluid Dynamics and Thermodynamics, 2007, pp. 1011-1020, March 5-9, Athens, Greece

Lien FS, Kalitzin G, *Computations of transonic flow with the ν^2-f turbulence model*, Int. J. Heat Fluid Flow 2001, 22(1):53-61, doi: 10.1016/S0142-727X(00)00073-4

Luo J, Razinsky EH, *Conjugate heat transfer analysis of a cooled turbine vane using the ν^2-f turbulence model*, J. Turbomach. 2007, 129(4):773-781, doi: 10.1115/1.2720483

Qureshi I, Beretta A, Chana K, Povey T, *Effect of aggressive inlet swirl on heat transfer and aerodynamics in an unshrouded transonic HP turbine*, J. Turbomach. 134(6), 061023 (Sep 04, 2012) (11 pages), doi:10.1115/1.4004876

Roache PJ, Kirti NG, White FM, *Editorial policy statement on the control of numerical accuracy*, J. Fluids Eng. 108, 1986, pag. 2, doi: 10.1115/1.3242537

Salvadori S, Montomoli F, Martelli F, Chana K S, Qureshi I, Povey T, *Analysis on the effect of a nonuniform inlet profile on heat transfer and fluid flow in turbine stages* J. Turbomach. 134, 011012 (2011) (14 pages); doi:10.1115/1.4003233

Takahashi T, Funazaki K, Salleh HB, Sakai E, Watanabe K, *Assessment of URANS and DES for prediction of leading edge film cooling*, ASME J Turbomach 2012, 134, Paper No. 031008, 13 pages, doi: 10.1115/1.4003054

Walters DK, Cokljat D, *A three-equation eddy-viscosity model for Reynolds-averaged Navier-Stokes simulations of transitional flow*, J Fluids Engineering 2008. 130(12), Paper No. 121401, 14 pages, doi: 10.1115/1.2979230

Wilcox DC, *Turbulence Modeling for CFD*, DCW Industries Inc. 1993